Determination of Particle Densities and Line Profiles in Plasmas by Resonance Interferometry: A Feasibility Study using Computer Simulated Refractivity Data

C. Haas, G. Pretzler [1], T. Neger, and H. Jäger

Institut für Experimentalphysik, Technische Universität Graz, Petersgasse 16, A-8010 Graz, Austria

Z. Naturforsch. **50a**, 902–914 (1995); received April 8, 1995

The principles of resonance interferometry are described with regard to two applications: High accuracy particle density determination within plasmas and interferometrical determination of spectral line profiles. The usability of this technique is investigated numerically, and physical limits are given for the regions in which resonance interferometry may be employed successfully. The discussion and the results are helt general for making it possible to decide whether or not to apply this method for an actual problem. An example (an object being longitudinally homogeneous with respect to the direction of light: end-on observation) shows how to use the presented results for calculating the detection limits of the method for a given object geometry.

1. Introduction

The sensitivity of interferometric measurements of phase objects can be strongly enhanced if one utilizes the strong refractive index variations in the nearest spectral vicinity of an atomic transition line. This technique, often referred to as resonance interferometry, has recently been applied to the optical investigation of gas flows (e.g. enhanced flow visualisation [1, 2]) and plasmas (e.g. determination of atomic particle densities [3]). In the spectral region of an atomic transition the refractivity (this is the quantity determined interferometrically) and the extinction coefficient (the quantity describing the absorption or emission line profile) of gaseous media are closely connected one to the other (see e.g. [4]). Therefore a further application of resonance interferometry could be the determination of line profiles and line widths. In this paper the properties of resonance interferometry shall be investigated generally, especially the conditions under which it is possible and may be favourable to employ this method for the determination of particle densities and line shapes. The purpose is to work out recipes when and when not to use resonance interferometry in practice.

The straightforward way for determining line shapes and particle densities is emission spectroscopy. However, if the object under investigation is partly optically thick, emission data are corrupted by self-absorption. In this case measurements can be done using absorption spectroscopy but, as will be demonstrated, the observed shapes of the absorption lines differ from the correct spectral profiles inside the object. What is more, the spatial distribution of the particle densities within most objects is a priori unknown and may well be asymmetrical, which makes the connection between measured and actual absorption profiles even more complicated. Especially with objects which are partially optically thick one has to face severe problems, because some spatial regions do not allow proper emission measurements due to self-absorption, while other regions do not show any measurable absorption effect.

Resonance interferometry offers a favourable way for investigating this kind of objects. Here the interesting internal quantity (refractivity) is connected linearly to the measured quantity (phase shift of light), no matter whether the object is optically thin or (partially) thick. Hence only one measuring method can be used regardless of the object. From the spectral course of the refractivity both the line shape and the particle density can be determined. However, problems arise if an object is totally optically thick. Then in the nearest spectral vicinity of a transition line the incident light intensity is (almost) totally absorbed. Therefore in this case interferometric measurements do not yield refrac-

[1] Present address: Max-Planck-Institut für Quantenoptik, Hans-Kopfermann-Straße 1, D-85748 Garching, email: gep@ipp-garching.mpg.de.

Reprint requests to Dr. G. Pretzler.

0932-0784 / 95 / 1000-0902 $ 06.00 © – Verlag der Zeitschrift für Naturforschung, D-72027 Tübingen

tivity data for the whole profile in the resonance region, but only at the wings up to a certain limit given by absorption. The main question for our investigations presented in this paper is whether and under which conditions it is possible to calculate the correct total line shape from erroneous data available only at the wings of a spectral line profile.

A brief discussion of the theory of refraction and absorption is given in Chapter 2. In Chapt. 3, the results of a feasibility and accuracy study are presented which was performed using computer simulated refractivity data. Different line shapes, particle densities, absorption conditions and measurement errors were simulated, thus yielding a wide survey. In Chapt. 4, these results are discussed and interpreted, which can be understood as kind of a recipe for experimentalists. The aim is to make it possible to estimate in advance whether the application of resonance interferometry to a special problem will be useful and which sensitivity is to be expected.

2. Theoretical Background

2.1 Refractivity and Extinction Coefficient

Since the full theoretical description of refraction and absorption within gaseous media would exceed the scope of this paper, we refer to the basic explications given in [4, 5, 6]. As shown in [4], in the spectral vicinity of an isolated atomic resonance transition the frequency dependence of the refractivity $n-1$ and of the extinction coefficient κ of a gas can be written as

$$n(\omega) - 1 = \frac{e^2}{4 \cdot m_e \cdot \varepsilon_0} \cdot \frac{N_i \cdot f_{ik}}{\omega_{ik}} \cdot \frac{\omega_{ik} - \omega}{(\omega_{ik} - \omega)^2 + (\gamma/2)^2}, \quad (1)$$

$$\kappa(\omega) = \frac{e^2}{4 \cdot m_e \cdot \varepsilon_0} \cdot \frac{N_i \cdot f_{ik}}{\omega_{ik}} \cdot \frac{\gamma/2}{(\omega_{ik} - \omega)^2 + (\gamma/2)^2}, \quad (2)$$

where N_i is the lower state particle density, f_{ik} the oscillator strength, ω_{ik} the resonance frequency, γ the decay rate, m_e the electron mass, e the electron charge and ε_0 the permittivity of vacuum.

If no particle interactions are considered, the decay rate γ results only from the finite lifetime of excited atomic states and is connected to the transition probability of the downward transition (see e.g. [6]). The linewidth resulting in this case (i.e. without considering any particle interactions) is called *natural linewidth.* The spectral profiles of $n-1$ and κ (see (1) and (2)), which are often referred to as Lorentz refractivity and absorption profiles, are plotted in Figure 2.1. It can easily be shown that the shape of these functions is determined by the decay rate γ. In the κ-profile γ is exactly the halfwidth (full width at half maximum, FWHM), in the $(n-1)$-profile it is the spectral separation of the two extremes.

In real gases and plasmas interactions between the particles lead to a broadening of the profiles. The most important effects are collisions and the influence of charged particles on the atomic energy levels (Stark effect). Both mechanisms shorten the lifetime of excited states and therefore increase the decay rate, but do not change the shape of the profiles, which are still of the Lorentz-type [4, 6, 7]. These so-called *homogeneous* line broadening effects lead to Lorentz profiles characterized by a larger halfwidth (or larger spectral separation of the extremes) compared to the natural linewith. This homogeneous linewidth (or decay rate γ) depends on the state of the surrounding medium. Especially in plasma physics different models have been developed for describing the dependence of γ on the plasma state which is mainly determined by the atom, ion and electron densities, pressure, collisional rates between the particles, kinetic temperature and degree of ionisation (see e.g. [7, 8, 9, 10]).

2.2 The Voigt Profile

A second broadening effect in plasmas is caused by the motion of the particles. Due to the Doppler effect the actual resonance frequency ω of a moving atom is shifted from the transition frequency ω_{ik} for a stationary particle. If the motion of the particles can be assumed to be thermal, their velocities have the Maxwellian distribution (see e.g. [11]). In this case the resulting distribution $g(\omega_{ik} - \omega)$ of the actual resonance frequencies ω is a Gaussian distribution around the resonance frequency ω_{ik} for motionless particles (see e.g. [12]), i.e.

$$g(\omega_{ik} - \omega) = \sqrt{\frac{2 \cdot \ln 2}{\pi}} \cdot \frac{1}{\gamma_D} \cdot \exp\left\{ -4 \cdot \ln 2 \cdot \frac{(\omega_{ik} - \omega)^2}{\gamma_D^2} \right\}. \quad (3)$$

In (3) γ_D is the halfwidth of the distribution function and is given by

$$\gamma_D = \frac{2 \cdot \omega_{ik}}{c} \cdot \sqrt{\frac{2 \cdot \ln 2 \cdot k_B \cdot T}{M}}, \quad (4)$$

where c is the velocity of light and M the particle mass.

Since this statistical shifting of the resonance frequency (often referred to as *inhomogeneous* line broadening or Doppler broadening) and the homogeneous broadening (see section 2.1) always occur simultaneously, the exact spectral profiles of the refractivity and the extinction coefficient are obtained by a convolution of the two Lorentz profiles with the Gaussian distribution function (3) [4, 6]. The convolution integrals are given by

$$n(\omega) - 1 = C \cdot \int_{-\infty}^{\infty} \frac{(\omega' - \omega)}{(\omega' - \omega)^2 + \gamma_L^2/4} \cdot \frac{2 \cdot \sqrt{\ln 2}}{\gamma_D \cdot \sqrt{\pi}} \cdot \exp\left\{ -4 \cdot \ln 2 \frac{(\omega' - \omega_{ik})^2}{\gamma_D^2} \right\} \cdot d\omega', \quad (5)$$

$$\kappa(\omega) = C \cdot \int_{-\infty}^{\infty} \frac{\gamma_L/2}{(\omega' - \omega)^2 + \gamma_L^2/4} \cdot \frac{2 \cdot \sqrt{\ln 2}}{\gamma_D \cdot \sqrt{\pi}} \cdot \exp\left\{ -4 \cdot \ln 2 \frac{(\omega' - \omega_{ik})^2}{\gamma_D^2} \right\} \cdot d\omega', \quad (6)$$

with

$$C = \frac{e^2 \cdot f_{ik} \cdot N_i}{4 \cdot m_e \cdot \varepsilon_0 \cdot \omega_{ik}}, \quad (7)$$

where γ_L is the former decay rate γ (in the following referred to as Lorentz-width) and γ_D is the halfwidth given by (4) (or Doppler-width).

Introducing the dimensionless variables

$$x = \frac{2 \cdot \sqrt{\ln 2}}{\gamma_D} \cdot (\omega_{ik} - \omega), \quad (8)$$

$$y = \frac{2 \cdot \sqrt{\ln 2}}{\gamma_D} \cdot (\omega_{ik} - \omega'), \quad (9)$$

$$a = \sqrt{\ln 2} \cdot \frac{\gamma_L}{\gamma_D} \quad (10)$$

and inserting them into (5) and (6) yields two integral expressions. After some elementary mathematical modifications these expressions can be identified as the real and the imaginary part of a representation of the complex probability function $W(z)$ for the complex upper half plane (see e.g. [13]). The function $W(z)$ is given by (see e.g. [14])

$$W(z) = e^{-z^2} \cdot \left[1 + \frac{2 \cdot i}{\sqrt{\pi}} \cdot \int_0^z e^{t^2} \cdot dt \right], \quad (11)$$

with

$$z = x + i \cdot a \quad (12)$$

and x and a from (8) and (10).

With this complex function the expressions for the refractivity $n-1$ and the extinction coefficient κ are represented in the form (see [2])

$$n(\omega) - 1 = \frac{e^2 \cdot \sqrt{\pi \cdot \ln 2}}{2 \cdot m_e \cdot \varepsilon_0} \cdot \frac{N_i \cdot f_{ik}}{\omega_{ik} \cdot \gamma_D} \cdot \mathrm{Im}[W(z)], \quad (13)$$

$$\kappa(\omega) = \frac{e^2 \cdot \sqrt{\pi \cdot \ln 2}}{2 \cdot m_e \cdot \varepsilon_0} \cdot \frac{N_i \cdot f_{ik}}{\omega_{ik} \cdot \gamma_D} \cdot \mathrm{Re}[W(z)]. \quad (14)$$

These convolved profiles are often referred to as *Voigt* profiles. Since the integral within the complex probability function $W(z)$ cannot be evaluated analytically, numerical methods must be applied (see e.g. [13, 15, 16] or tabulated values of the function (e.g. [14]) are employed. The total halfwidth γ_V (FWHM) of a Voigt profile can be approximated [17] by

$$\gamma_V = \frac{1}{2} \cdot \left(\gamma_L + \sqrt{\gamma_L^2 + 4 \cdot \gamma_D^2} \right). \quad (15)$$

The variable x (8) is equivalent to the nondimensional frequency corresponding to the resonance frequency ω_{ik}, whereas the parameter a, (10) and (12), is determined by the ratio γ_L/γ_D and influences the shape of the profiles. To emphasize this fact, in Fig. 2.2 some extinction profiles are plotted with different ratios γ_L/γ_D but equal halfwidths. It can be seen that the dotted extinction profile ($\gamma_L/\gamma_D = 10$) is very similar to the pure Lorentz profile in Figure 2.1 (b). For this and larger ratios (called *Lorentz region* in the following) there is no significant influence of the Doppler-width γ_D on the shape of the profile. On the other hand, if γ_L/γ_D is equal to 0.1 or smaller (*Doppler region*), the extinction profile is almost only a Gaussian distribution. Besides these two extremes there is a wide *intermediate region* with ratios of γ_L/γ_D from 0.1 to 10. Here both parameters influence the shape of the extinction profile, which is some sort of a "mixture" of the Gaussian and the Lorentzian type.

In Figure 2.3 the corresponding refractivity profiles are shown. Again, the profile with $\gamma_L/\gamma_D = 10$ is almost indentical to the pure Lorentz refractivity profile (Figure 2.1 (a)). The larger the influence of the Doppler-width γ_D, the higher the peak values and the steeper the slopes. However, there is one major difference between the extinction and the refractivity line profiles: While different extinction profiles remain different at the wings (cf. Fig. 2.2: the difference is visible at least up to a frequency shift of four linewidths) all the re-

fractivity profiles converge to one common profile (cf. Fig. 2.3: the differences almost vanish at a frequency shift of two linewidths) which can be described by Sellmeier's formula (see e.g. [5])

$$n(\omega) - 1 = \frac{e^2}{2 \cdot \varepsilon_0 \cdot m_e} \cdot \frac{N_i \cdot f_{ik}}{\omega_{ik}^2 - \omega^2}. \tag{16}$$

This formula is a simplification of (1) neglecting the influence of the decay rate γ. Therefore special properties of the profile, which are mainly introduced through γ, are not included in (16).

2.3 Determination of Plasma Parameters

Use of (13) and (14) makes it possible to calculate the spectral course of the refractivity $n-1$ and of the extinction coefficient κ of gaseous media, taking into account all homogeneous line broadening mechanisms and the Doppler broadening simultaneously. However, the problem in the case of resonance interferometry and spectroscopy is put the other way round: Some quantities (not even $n-1$ and κ directly, see below) are measured spectrally resolved, and from these the particle density N_i and the linewidths γ_L and γ_D shall be calculated (and as much as possible further information about the investigated object from these). This can be done by fitting the measured data to (13) or (14) by some non-linear fitting algorithm (see Section 3.1).

However, this is not the whole problem. The refractivity $n-1$ and the extinction coefficient κ are local quantities, which means that normally they are constant only within infinitesimal volume elements of an object. Optical measurements can only yield integral data along the light path through an object. In the case of interferometry and absorption spectroscopy, the measured quantities are the phase shift $\delta\varphi(\omega)$ and the transmitted light intensity $I(\omega)$, which are connected to the microscopic quantities $n(\omega)$ and $\kappa(\omega)$ by integrals (cf. [4]):

$$\delta\varphi(\omega) = \frac{\omega}{c} \cdot \int_L (n(\omega) - n_0)\,\mathrm{d}l, \tag{17}$$

$$I(\omega) = I_0 \cdot \exp\left\{-\frac{2 \cdot \omega}{c} \cdot \int_L \kappa(\omega)\,\mathrm{d}l\right\}, \tag{18}$$

where n is the refractive index within the object, n_0 the constant refractive index in the reference path of an interferometric setup, L the geometrical path length of the object, l the direction of light and I_0 the incident light intensity.

Equation (17) describes the situation for interferometric measurements and shows a *linear* connection of the measured quantity $\delta\varphi$ and the corresponding local quantity $n-1$. In general, the refractivity cannot be obtained from one single measured phase shift because normally $n-1$ will have a spatial distribution. Therefore, in general tomographic methods must be used (see e.g. [18, 19]) for determining the refractivity at a certain point within the object. This problem is beyond the scope of this paper, therefore only a special case shall be discussed here, i.e. an object which is homogeneous in the direction l of light. Then the integral in (17) degenerates to a multiplication by the path length L and $n-1$ can easily be calculated. Due to the linearity of (17), the spectral profiles of $\delta\varphi$ and of $n-1$ are equally shaped, no matter whether the object is optically thin or not. This shows that interferometric measurements are never influenced by the object's optical thickness.

Equation (18), describing the case of absorption measurements, is more complicated because here the connection between measured and local quantities ($I(\omega)$ and κ) is exponential. Even for homogeneous objects (again the integration is replaced by the multiplication by L) the measured and the local spectral profiles may differ. If the exponent in (18) (in the homogeneous case this is $(2\,\omega/c)\,\kappa(\omega)\,L$), which is commonly referred to as *optical depth* of a plasma, is small compared to 1, the exponential function may be expanded into a power series which can cut be off after the linear term. In this case, the relation between I and κ is linear, and therefore the intensity profile has the same shape and halfwidth as the profile of the extinction coefficient. If this linear approximation is valid, the plasma is called to be *optically thin.* However, if the optical depth is equal to or larger than 1, the terms of higher order in the series expansion are no more negligible. In this case, the plasma is said to be *optically thick* and the shape of the intensity profile differs from the corresponding extinction profile (see examples in Figure 2.4). For obtaining the extinction profile, the function

$$\phi(\omega) = \ln\left(\frac{I(\omega)}{I_0}\right) = -\frac{2\,\omega}{c} \cdot \int_L \kappa(\omega)\,\mathrm{d}l \tag{19}$$

must be calculated. $\phi(\omega)$ is linearly connected to $\kappa(\omega)$ and therefore can serve as the basis for tomographical reconstruction of κ for asymmetrical objects and is proportional to κ for homogeneous objects. Like the

interferometrically measured quantity $\delta\varphi$, the function $\phi(\omega)$ is independent of the object's optical depth.

With both methods, interferometry and absorption measurements, there are problems investigating optically thick objects, because it may happen that practically no light is transmitted in the spectral center of the actual transition line (see Figure 2.4). The function $\phi(\omega)$ is not defined in this case, but there may also be difficulties in using the transformation (19) for small intensities, because then the measurement errors are strongly enlarged by the logarithm. Although the phase shift $\delta\varphi$ does not depend on absorption, it cannot be measured if absorption is total because no light remains to form interference fringes. Therefore in this case the $\delta\varphi(\omega)$ profile can only be measured at the spectral wings, and consequently the $n(\omega)$ profile, too.

Up to now, the discussion was led parallel for interferometry and absorption measurements. Now we want to focus only on resonance interferometry. In the following chapter we will assume that the refractivity profile $(n(\omega)-1)$ can be measured for one spatial point within an object (except the absorption region in the spectral line center). From these data the parameters (particle density N_i, Lorentz-width γ_L and Doppler-width γ_D) shall be calculated. The question is, which parts of the profile must be measured for a successful calculation of these parameters by a least-squares-fit. The following chapter is devoted to a systematic numeric analysis of the feasibility of such a fit as well as of the accuracy of the determined parameters, both under different simulated measurement conditions.

3. Accuracy Analysis

3.1 Method

The basic problem of resonance interferometry is shown in Figure 3.1: The refractivity can only be measured at the spectral wings of the profile and the innermost measurable point has a spectral difference $d\omega$ to the line center. The question is how large this difference may be if the profile shall be calculated correctly. What makes the problem more complicated, the measured points have a certain measurement error, and the exact position of the line center ω_{ik} is normally not known precisely.

The feasibility of least-square-fitting refractivity profiles and the accuracy of the fitted plasma parameters N_i, γ_L and γ_D under these conditions were analysed using computer simulated refractivity data. To obtain general results, some parameters, namely the plasma conditions, the measurement error, the number of data points and their spectral position in relation to the resonance frequency were varied. In the following we briefly describe the procedure of data simulation.

First of all, sets of values for the plasma parameters N_i, γ_L and γ_D were chosen in the physical range of low temperature plasmas. This means particle densities of the investigated species from 10^{16} to 10^{24} m^{-3}, Lorentz-widths from 10 MHz (which is the order of magnitude of the natural linewidths for many transitions) to 100 GHz, and Doppler-widths corresponding to a temperature range from 300 K to 30000 K (cf. (4)). By choosing values for these parameters, a certain refractivity profile is defined (according to (13)) which is assumed to be valid within one volume element of a plasma.

From this simulated model function, a particular number of spectral data points were selected. In general, 20 points were used (a number which seems to be experimentally achievable without too much efforts), but the number was varied between 5 and 30. For simulating optically thick plasmas (see Chapt. 2.3), no data points were taken from a certain spectral region around the resonance frequency. The frequency detuning $d\omega$ of the innermost data point from the line center (see Figure 3.1) was varied from zero up to about three linewidths γ_V (see (15)), the spectral distance between the points was chosen between 1/5 and 1/2 linewidths γ_V. Measurement errors were simulated by artificial noise following a Gaussian distribution of which the standard deviation was varied for studying the influence of different measurement errors.

A large number of data sets with different plasma parameters, measurement errors and frequency positions of the data points was generated, and each set of data points was fitted to (13). Since this expression is non-linear with respect to the parameters γ_L and γ_D, the Levenberg-Marquardt-method [20, 21] was used, which is a standard non-linear least-squares algorithm. The fitted values of the three parameters N_i, γ_L and γ_D were compared with the chosen parameters, which allows an easy judgement of the quality of the results. Furthermore, the applied fit algorithm yields the statistical errors of the fitted parameters, thus allowing the estimation of the method's sensitivity under different conditions. The results of this study are presented in the following section.

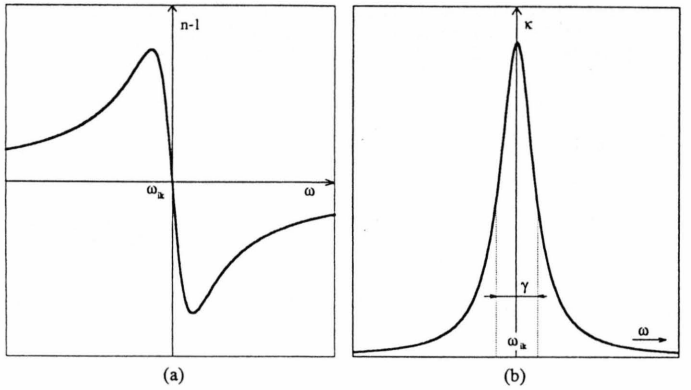

Fig. 2.1. Lorentz profiles for an isolated transition at the frequency ω_{ik}. (a) Profile of the refractivity $n-1$, (b) profile of the extinction coefficient κ.

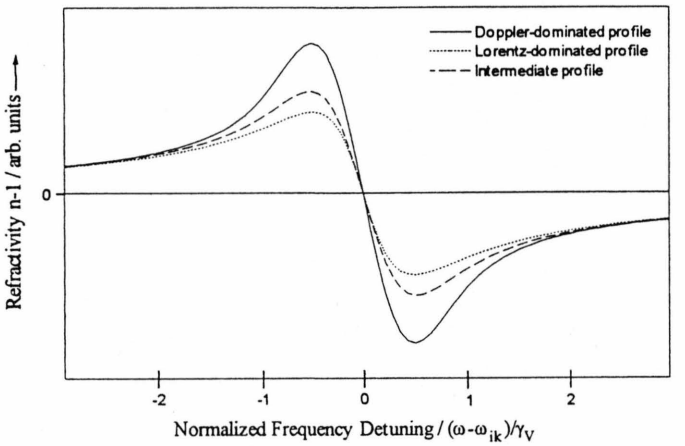

Fig. 2.3. Spectral profiles of the refractivity $n-1$ (Voigt profile, see (13)) for different ratios γ_L/γ_D, normalized to the same linewidth γ_V (FWHM). The curves represent ratios of 0.1 (solid), 1 (dashed) and 10 (dotted).

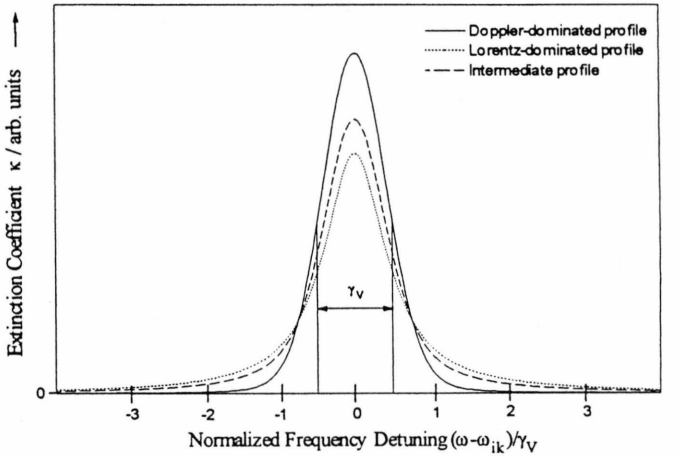

Fig. 2.2. Spectral profiles of the extinction coefficient κ (Voigt profile, see (14)) for different ratios γ_L/γ_D, normalized to the same linewidth γ_V (FWHM). The curves represent ratios of 0.1 (solid), 1 (dashed) and 10 (dotted).

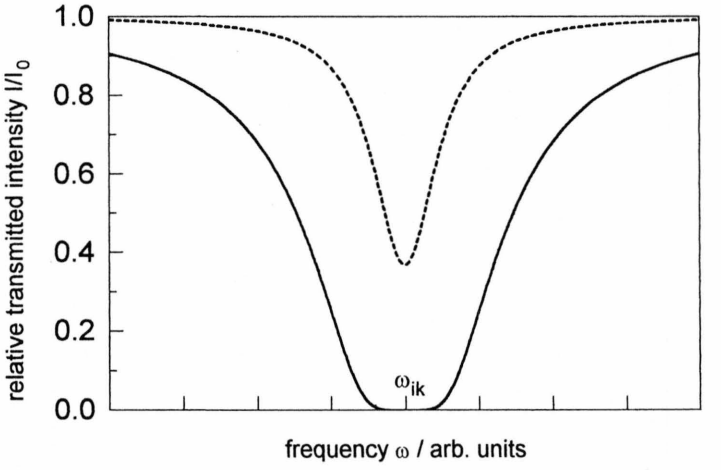

Fig. 2.4. Examples for the spectral profiles of light (intensity I) transmitted through longitudinally homogeneous plasma columns in the spectral vicinity of a resonance frequency ω_{ik} (see (17)). Dashed curve: optically thin plasma, solid curve: optically thick plasma.

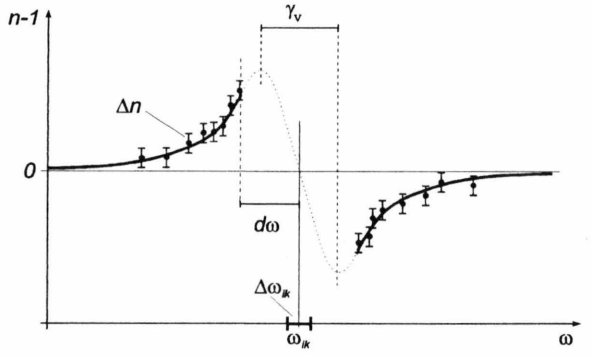

Fig. 3.1. On the problem of experimentally determining a refractivity pofile $(n-1)$: Measured refractivity values (error Δn) are available only down to a minimum spectral distance $d\omega$ to the line center ω_{ik} (which has a position uncertainty of $\Delta\omega_{ik}$ itself) due to absorption in the central spectral region. The question is how well the profile (halfwidth γ_V) can be determined by fitting the measured data to the Voigt profile (13).

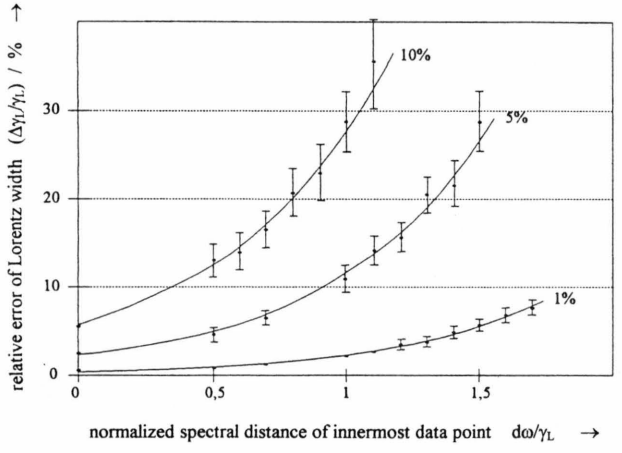

Fig. 3.3. Relative error $\Delta\gamma_L/\gamma_L$ of the fitted Lorentz-width as a function of the spectral detuning $d\omega$ of the innermost data point (in units of the given Lorentz-width γ_L) for three different maximum measurement errors (1%, 5% and 10% of the peak-value of the refractivity profile). The diagram is valid for the Lorentz region.

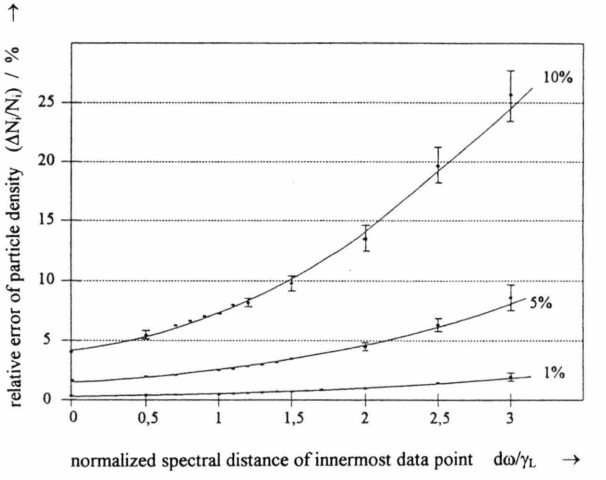

Fig. 3.2. Relative error $\Delta N_i/N_i$ of the fitted particle density as a function of the spectral detuning $d\omega$ (see Fig. 3.1) of the innermost data point (in units of the given Lorentz-width γ_L) for three different maximum measurement errors (1%, 5% and 10% of the peak-value of the refractivity profile). The diagram is valid for the Lorentz region (ratios $\gamma_L/\gamma_D > 10$).

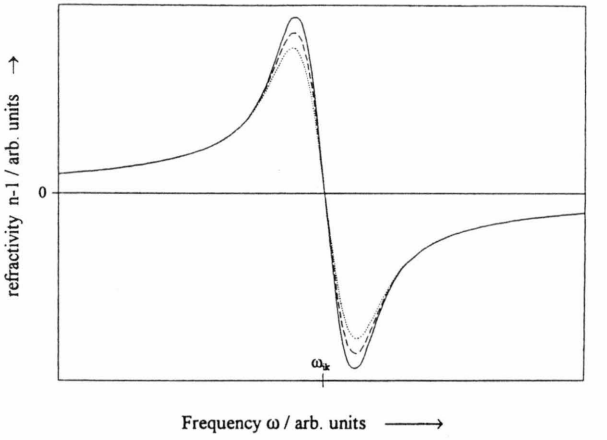

Fig. 3.4. Comparison of three Doppler-dominated refractivity profiles with different ratios γ_L/γ_D (Solid curve: $\gamma_L/\gamma_D = 1/100$; Dashed curve: $\gamma_L/\gamma_D = 1/10$; Dotted curve: $\gamma_L/\gamma_D = 1.5$, γ_D and the particle density N_i are the same for all three curves). The only influence of the different Lorentz widths is in the spectral vicinity of the extremes.

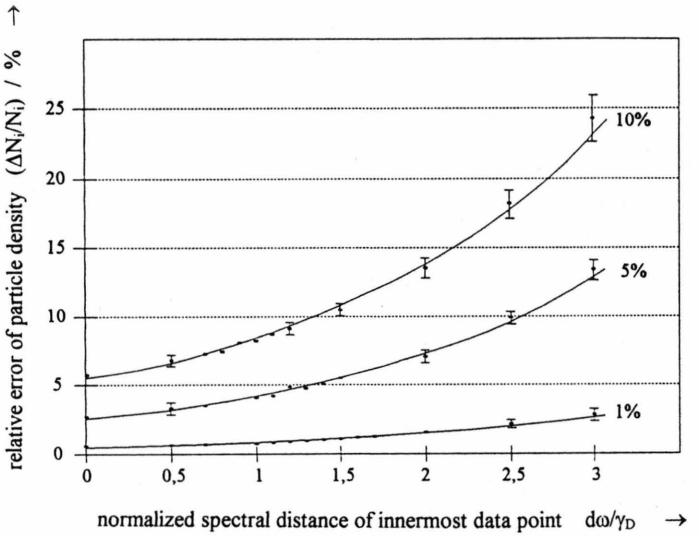

Fig. 3.5.

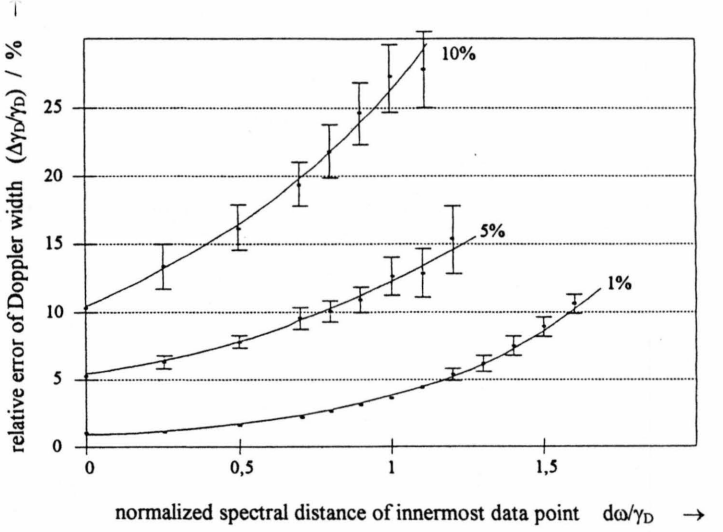

Fig. 3.6.

Fig. 3.7.

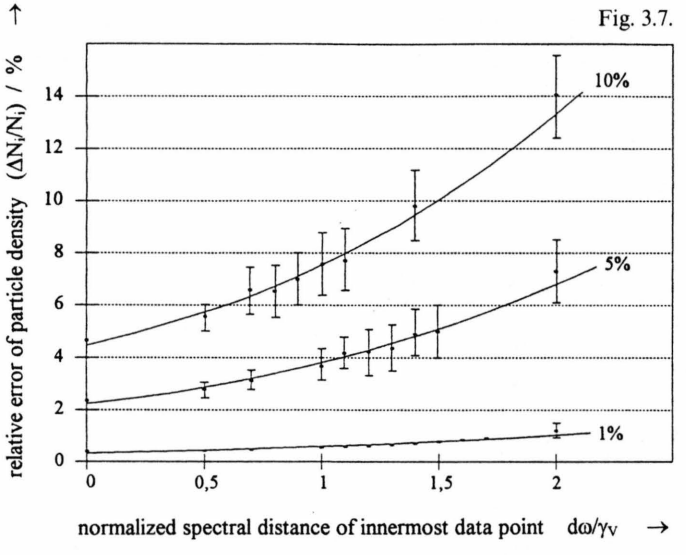

Fig. 3.5. Relative error $\Delta N_i/N_i$ of the fitted particle density as a function of the spectral detuning $d\omega$ of the innermost data point (in units of the given Doppler-width γ_D) for three different maximum measurement errors (1%, 5% and 10% of the peak-value of the refractivity profile). The diagram is valid for the Doppler region (ratios $\gamma_L/\gamma_D < 0.1$).

Fig. 3.6. Relative error $\Delta\gamma_D/\gamma_D$ of the fitted Doppler-width as a function of the spectral detuning $d\omega$ of the innermost data point (in units of the given Doppler-width γ_D) for three different maximum measurement errors (1%, 5% and 10% of the peak-value of the refractivity profile). The diagram is valid for the Doppler region.

Fig. 3.7. Relative error $\Delta N_i/N_i$ of the fitted particle density as a function of the spectral detuning $d\omega$ of the innermost data point (in units of the given Voigt-width γ_V) for three different maximum measurement errors (1%, 5% and 10% of the peak-value of the refractivity profile). The diagram is valid for the intermediate region. $\gamma_L/\gamma_D \approx 1$.

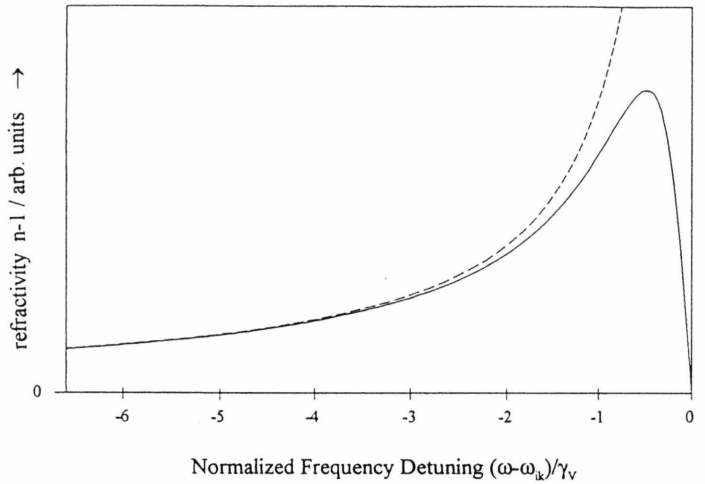

Fig. 4.1. Comparison of the Voigt refractivity function (13) with a ratio $\gamma_L/\gamma_D = 1$ and Sellmeier's formula (18). It can be seen that the two functions converge for frequency detunings of more than two linewidths of the Voigt profile.

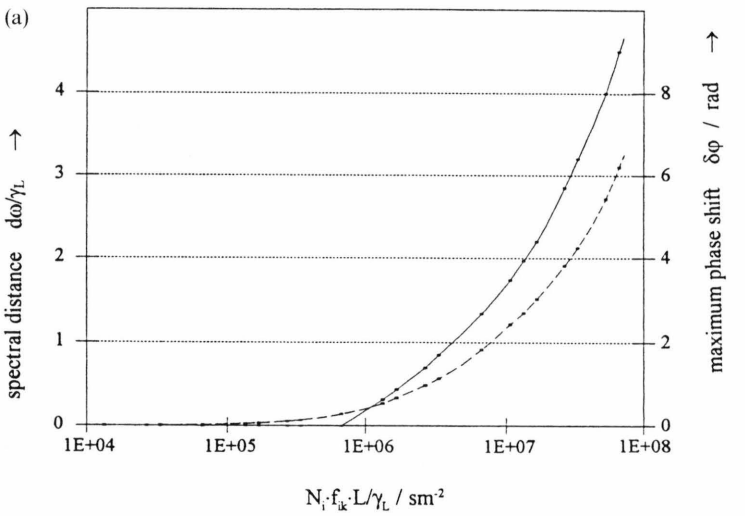

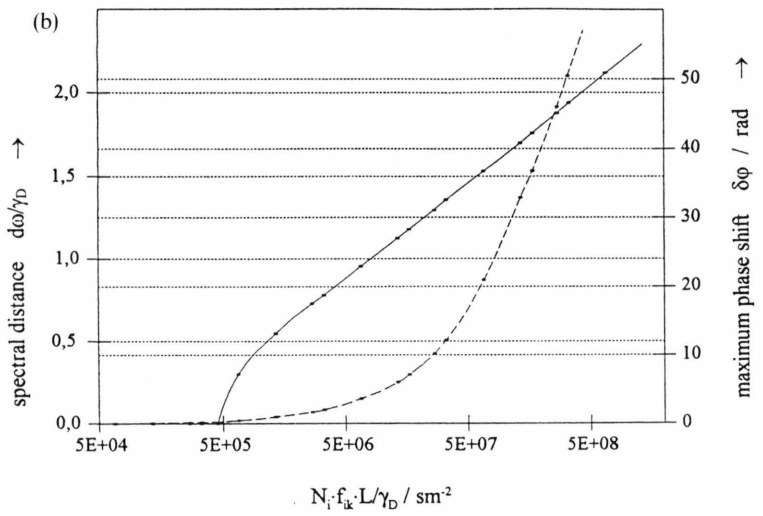

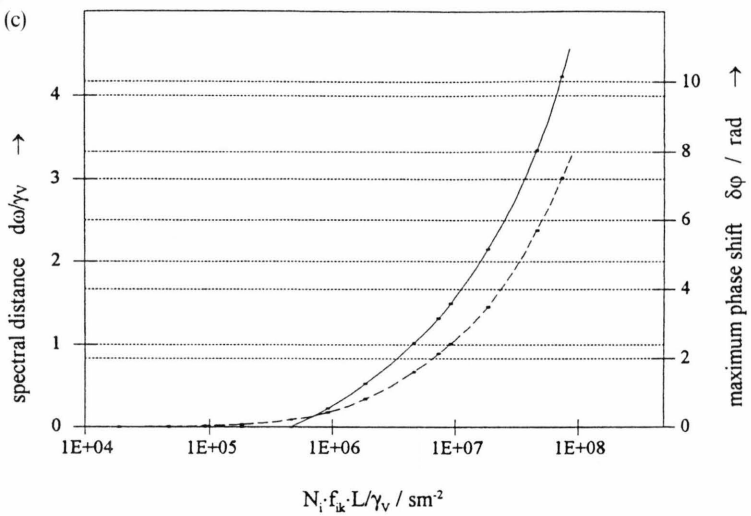

Fig. 4.2 Effect of a homogeneous object on the transmitted light in the spectral vicinity of a transition line. (a) Lorentz region, (b) Doppler region, (c) intermediate region (ratio $\gamma_L/\gamma_D = 2$). Solid: Frequency detuning $d\omega$ of the 75 percent absorption frequency, dashed: maximum phase shift $\delta\varphi$ of the transmitted light, both as a function of the parameter $N_i f_{ik} L/\gamma$ (a measure for the optical thickness). Resonance interferometry is only possible in the region where the phase shift is detectably high but $d\omega$ is not too high (cf. Figs. 3.2 to 3.7).

3.2 Results

General Results

The investigations showed that the number of data points does not critically influence the results of the fit as long as at least about 12 points are used. Further decreasing of the number of data points leads to rapidly increasing fitting errors.

The dependence of the fitting errors on the standard deviation of the simulated measurement errors proved to be linear for the case of optically thin objects (data points at the center available) and exponential for optically thick objects (no data points in the central spectral region of the line).

In practice the exact spectral position ω_{ik} of the line center is often unknown with respect to the measured profile. It was shown numerically that an error up to $\Delta\omega_{ik}=\gamma_V/10$ does not produce a significant increase of the fitting errors.

The results for the accuracy of the fitting results proved to be characteristically dependent on the profile shapes. We found it useful to define three separate regions determined by the ratio γ_L/γ_D in the Voigt function (see Sect. 2.2): the Lorentz region (ratios $\gamma_L/\gamma_D \geq 10$), the Doppler region (ratios $\gamma_L/\gamma_D \leq 0.1$), and the intermediate region between these two extremes (ratios $0.1 \leq \gamma_L/\gamma_D \leq 10$).

Lorentz Region

In this region the Doppler-width γ_D does not influence the profile shape (see Sect. 2). From this it is obvious that in the Lorentz region γ_D cannot be determined properly by the least-squares fit. Nevertheless, the other two fit parameters, i.e. the lower state particle density N_i and the Lorentz-width γ_L, are calculated quite well, even with large measurement errors and optically thick objects. In the Figs. 3.2 and 3.3 the relative errors of these parameters are shown. The dependence of these errors on the spectral distance $d\omega$ (see Fig. 3.1), which is a measure for the optical thickness of the object, is nearly, exponential, but not too steep. Thus the Lorentz-width γ_L can be calculated accurately up to a distance of $d\omega = 1.5\,\gamma_V$ (this means that a "black zone" in the spectral line center is allowed which is three times the FWHM) and the particle density N_i up to at least $d\omega = 3\,\gamma_V$.

The error bars in the Figs. 3.2 and 3.3 (and in all the following figures) show the result of a statistical analysis of the fit errors. The simulation was done repeatedly under the same plasma conditions (ratio γ_L/γ_D as well as the measurement limit due to optical depth), but using different sets of simulated statistical measurement errors (with the same standard deviation) of the refractivity data. The values shown in the figures are the mean values of at least six different calculations; the error bars represent the resulting standard deviations.

Doppler Region

These are the profiles of which the shape is only very weakly influenced by the Lorentz-width γ_L. As shown in Fig. 3.4, profiles with different ratios γ_L/γ_D, but equal particle density and Doppler-width differ only in the immediate spectral range of the profile extremes. Therefore correct fit results for the Lorentz-width can only be obtained if measured data points are available in the spectral vicinity of the extremes of the refractivity profile. However, even then the fit results for γ_L proved to be unstable and critically influenced by measurement errors. For practical applications, especially with optically thick objects, it must be stated that normaly it will not be possible to obtain reliable results for the Lorentz-width in the Doppler region.

The results for the fit quality of the other two parameters are shown in the Fig. 3.5 (Doppler-width γ_D) and Fig. 3.6 (particle density N_i). They are similar to those in the Lorentz region. The Doppler-width γ_D is fitted reliably up to a distance $d\omega = 1.5\,\gamma_V$, and the particle density N_i up to about $d\omega = 3\,\gamma_V$.

Intermediate Region

This is the region where the profile shape depends both on the Lorentz- and on the Doppler-widths very sensitively. Nevertheless, the numerical calculations showed that the Lorentz- and the Doppler-widths can only then be determined accurately, if data points are given nearly up to the spectral positions of the extremes of the refractivity profile. Generally, the larger of the two quantities is calculated more accurately (because its influence on the line shape is more important and therefore more easily found by the fit algorithm). If they are about equal, the fit fails for both parameters γ_L and γ_D if the distance of the innermost point to the central frequency is greater than about 70% of the linewidth γ_V. This result can be explained by the fact that the profile differences are mainly in the

spectral region of the extremes (see Fig. 2.3) and therefore data points must be available near the extremes for being able to distinguish between different profiles. Thus the correct determination of both linewidths is restricted to objects which are optically thin or at least not too much optically thick.

The particle density N_i can be evaluated for a larger group of objects. The results are plotted in Fig. 3.7 and show that N_i is calculated reliably up to a distance of $d\omega = 2\gamma_V$ of the innermost data point from the line center. This is a smaller distance than for the Lorentz and the Doppler region. The reason is that the fit results for γ_L and γ_D become very incorrect when the distance of the innermost data point is larger than one and a half linewidths. Since all three fit parameters are correlated to each other (correlation coefficients were found to be greater than 0.5 in general), this affects the fit result for the particle density, and consequently the fit fails more easily than in the two other profile regimes.

4. Discussion of the Results

4.1 Failure of the Fit

As shown in Sect. 3.2, a reliable calculation of the line shape is possible only in a certain range of optical thickness. Beyond this range the fit quality for the linewidths decreases dramatically, but nevertheless the particle density can be determined quite well. In this section the behaviour of the fit shall be discussed for cases when it fails partly or totally.

Why can the correct profile in the intermediate region be calculated only if it is possible to measure close to the extremes? The answer is shown in Figure 2.1. If the data points are lying too far outwards, they are in a region where different profiles have different smaller than the measurement error. It is principially impossible to decide which out of a lot of profiles is the correct one if all of them are the same in the measured region.

And why is there a limit for an object's optical thickness if the Lorentz-width shall be calculated in the Lorentz region? Here the Doppler-width plays no role, but nevertheless the effect is the same: Profiles with a very different Lorentz-width coincide at the wings beginning at a certain point, therefore with points measured only in the outer spectral region a decision between different profiles is impossible.

In the previous chapter it was discussed that the least-squares-fit of refractivity data in the spectral region of an isolated atomic transition frequency fails if the innermost data point lies more than a certain distance away from the line center. This distance is different for the three fit parameters and depends on the profile region, i.e. on the ratio γ_L/γ_D. On the other hand, the simulations showed that the particle density can be determined much better than the two linewidths, even in those cases when the linewidths are pretty wrong. The reason for this fact is that the quantity N_i appears as a linear factor in the refractivity function and therefore influences the whole profile in the same way. The points on the line wings do not carry sufficient information on the shape of the profile, but enough about the particle density. In the spectral region of the line center, the refractivity is dominated by the resonant characteristics of the atomic species, whereas in outer spectral regions the influence of the line shape decreases and the refractivity profile is well-described by Sellmeier's formula (16). Here the particle density is still linearly connected to the refractivity (and therefore can be determined from measurements in this spectral region), while the linewidths are not even mentioned. In Fig. 4.1 the transition from the resonant profile into Sellmeier's formula is shown for a profile with a ratio $\gamma_L/\gamma_D = 1$.

Nevertheless, the least-squares fit of the particle N_i to the Voigt-profile fails for distances $d\omega$ of more than three linewidths. This is caused by the fact that for such conditions the fit result for the parameters γ_L and γ_D are already that wrong that the stability of the fit for N_i is influenced, too, because of the correlation of the three fitting parameters (see above). The better way in the case of a failure of the fits for the linewidths is to calculate the particle density from a fit to Sellmeier's equation.

4.2 Applications

The applicability of resonance interferometry follows directly from the results presented in Chapter 3. First of all the determination of particle densities is possible for any optical depth of the object under investigation, even if it is largely optically thick. This is the most significant advantage of this resonant-interferometric method, in contrast to spectroscopic techniques.

Restricted to objects which are not too much optically thick the method allows the determination of the

shape of the refractivity profile, and from this (with the determined parameters N_i, γ_L and γ_D) the calculation of the corresponding absorption profile (cf. (14)). Thus it is possible to obtain the correct local line profiles even of objects of which one would obtain wrong profile shapes using spectroscopic methods due to the optical thickness. In this way, by means of interferometric measurements spectroscopic data can be obtained which are not affected by effects of the optical depth.

The interferometric determination of the linewidths has one more consequence for plasma physics. In the region of Lorentz-type profiles, the correct determination of the Lorentz-width γ_L is possible even if a plasma is optically thick. With this correct linewidth, conclusions on the plasma state can be made because the homogeneous linewidth depends on parameters like pressure, collisional rates, or the degree of ionisation (see Section 2). In the Doppler region, the correct fit results for the Doppler-width γ_D allow the determination of the kinetic temperature of one selected particle species. If the plasma is in the local thermal equilibrium (LTE), this temperature allows for the calculation of other plasma parameters like population densities using e.g. the Boltzmann distribution or Saha's equation. Only in the intermediate region the application of resonance interferometry to profile measurements (and the calculation of subsequent plasma parameters) is restricted to nearly optically thin plasmas. In each case the method can be applied for the determination of the densities of atomic particles without any doubts concerning optical thickness.

4.3 Numerical Example for a Homogeneous Object

Homogeneous plasmas are the most simple objects for experimental plasma diagnostics (see Section 2.3). In this section we will give a numerical example simulating interferometric measurements from a homogeneous object. The aim is to show the limits of this measurement technique under different plasma conditions. Although most real plasmas show other than homogeneous geometry, this example allows to obtain some general statements about the experimental conditions for investigating plasmas by means of resonance interferometry.

We started from the assumption that interferometric measurements are feasible if at least 25% of the incident light is transmitted through the object. This is a rough estimation justified by experimental experience and may be decreased by experimental measures. By inserting (14) into (18) and replacing the integration by a multiplication (due to the object's assumed geometrical homogeneity), that frequency was calculated for which 75% of the incident light are absorbed. This gives an approximation for the parameter $d\omega$ (spectral detuning of the innermost measurable data point from the the line center, see Figure 3.1). Next, the maximum expectable phase shift $\delta\varphi$ was calculated using (17) and (13) (the reference refractive index n_0 was assumed to be 1). This maximum phase shift will occur either at the frequency of the innermost data point (for $d\omega > \gamma$, see Fig. 3.1) or at the refractivity maximum (for $d\omega < \gamma$) and defines whether the sensitivity of the interferometric detection is sufficient for an accurate measurement. To get a parameter-free presentation, the results are plotted dependent on the factor $N_i f_{ik} L/\gamma$.

The results for the Lorentz region are shown in Figure 4.2 (a). For optically thin objects (left region, where the solid line does not appear) the maximum phase shift is extremely small, which demands extremely high sensitivity for the interferometric measurements. If the absorption limit is at about one linewidth from the center (limit for the determination of γ_L, see Section 3.2), the maximum phase shift is about 2 rad (and therefore well detectable), and for an absorption limit of 3 linewidths (limit for determination of N_i by fitting the Voigt-profile), $\delta\varphi$ is about 4 rad. Figure 4.2 (a) allows the calculation of the physical detection limits: Assuming for example a typical Lorentz-linewidth of 50 GHz, the upper limit for the interferometrical determination of the line profile is $N_i f_{ik} L \approx 5 \cdot 10^{17}\,\mathrm{m}^{-2}$, the upper limit for the particle density determination is $N_i f_{ik} L \approx 2 \cdot 10^{18}\,\mathrm{m}^{-2}$.

The results for the Doppler region are displayed in Fig. 4.2 (b) and are even more promising. At the limit for determining the Doppler-width, the maximum phase shift is 20 rad, at the limit for the particle density, the phase shift is greater than 100 rad (which is rather much for most interferometric techniques). With a typical Doppler linewidth ($\gamma_D \approx 2$ GHz) the upper limit for determining the profile is $N_i f_{ik} L \approx 10^{18}\,\mathrm{m}^{-2}$, and for determining the particle density it is $N_i f_{ik} L \approx 10^{19}\,\mathrm{m}^{-2}$.

In the intermediate region the results appeared to depend on γ_L/γ_D. Therefore we cannot present a diagram which is valid for the whole region. As an example, Fig. 4.2 (c) shows the results for $\gamma_L/\gamma_D = 2$. With a typical Voigt-width γ_V of 5 GHz, the measurement

limit for the determination of the two linewidths (75 percent absorption at a frequency shift of slightly more than half a linewidth, see section 3.2) and subsequently for the profile is found to be $N_i f_{ik} L \approx 10^{16}$ m^{-2} (with a corresponding phase shift of about 1 rad), whle the particle density can be evaluated correctly up to $N_i f_{ik} L \approx 10^{17}$ m^{-2} (phase shift is about 3 rad).

4.4 Conclusions and Outlook

The presented results show that, within certain limits, resonance interferometry can be useful tool in plasma diagnostics. First the method is useful for a highly accurate determination of ground state particle densities of certain atomic species regardless of optical depth. Second in a certain regime of plasma objects (in short objects which are optically not too thick) the method can be employed for determining the refractivity and extinction profiles of a transition line without perturbation by effects due to optical depth. There are restrictions concerning the types of objects to be investigated by this method. There is always a lower limit defined by the sensitivity of the interferometric detection of phase shifts and an upper limit given by measurement errors and undistinguishability of different profiles. These limits can be estimated using the results of Sect. 3.2, like it was shown in Section 4.3. Therefore an experimentalist can judge in advance whether the employment of resonance interferometry may be useful for a special problem.

Especially highly accurate interferometric methods seem to be suited for application in connection with resonant techniques, e.g. heterodyne holographic interferometry (e.g. [3]). Then the small measurement errors will help to extend the region where resonance interferometry can be applied. As pointed out in Sect. 2.3, one main problem is the spatial distribution of all the physical quantities, including the linewidths γ_L and γ_D. Therefore, for a diagnostic system yielding spatially resolved results the described resonant-interferometric technique must be combined with tomographic methods, like it was tried in [3].

Generally, resonance interferometry appears to be the "missing link" between the region of optically thin objects (where spectroscopic methods are used) and optically very thick objects (the region of classical spectro-interferometry or absorption measurements). The efforts for performing this technique might be large (e.g. tunable dye-lasers must be used for achieving the high spectral resolution), but as was shown in this paper, the achievable results are accurate and reliable.

[1] G. Blendstrup, D. Bershader, and L. Langhoff, J. AIAA **6,** 1106 (1978).
[2] E. Kügler and D. Bershader, Experiments in Fluids **1,** 1 (1983).
[3] J. Woisetschläger, H. Jäger, H. Phillip, G. Pfeifer, and T. Neger, Phys. Lett. A **152,** 42 (1991).
[4] A. P. Thorne, Spectrophysics, Chapter 8: Width and Shape of Spectral Lines, Chapter 9: Emission and Absorption of Line Radiation, Chapman & Hall, London 1974.
[5] R. W. Ditchburn, Light, Chapter 15: The Electromagnetic Theory of Absorption and Dispersion, 3rd edition, Academic Press, London 1976.
[6] A. E. Siegman, Lasers, Chapter 2: Stimulated Transitions: The Classical Oscillator Model, Chapter 3: Electric Dipole Transitions in Real Atoms, University Science Books, Mill Valley Ca. 1986.
[7] W. Lochte-Holtgreven (ed.), Plasma Spectroscopy, Chapter 2: Interpretation of Line Broadening and Line Shift (by G. Traving), North-Holland, Amsterdam 1968.
[8] H. R. Griem, Plasma Spectroscopy, Chapter 4: Linebroadening Calculations, McGraw-Hill, New York 1964.
[9] A. Unsöld, Physik der Sternatmosphären, Teil IV: Physikalische Grundlagen der Theorie der Fraunhofer-Linien, Springer, Berlin 1955.
[10] G. Traving, Über die Theorie der Druckverbreiterung von Spektrallinien, Verlag G. Braun, Karlsruhe 1960.
[11] L. D. Landau and E. M. Lifschitz, Lehrbuch der theoretischen Physik Band V: Statistische Physik, Kapitel III, §29: Maxwellsche Verteilung, Akademie-Verlag, Berlin 1971.
[12] W. Demtröder, Laserspektroskopie, Kapitel 3.2: Doppler-Verbreiterung, Springer, Berlin 1991.
[13] W. Armstrong, J. Quant. Spectrosc. Radiat. Transfer **7,** 62 (1962).
[14] M. Abramowitz and I. A. Stegun, Handbook of Mathematical Functions, Chapter 7: Error Function and Fresnel Integrals, Dover Publications, New York 1965.
[15] J. Humlicek, The Voigt Function and its Derivatives, J. Quant. Spectrosc. Radiat. Transfer **21,** 309 (1979).
[16] J. Humlicek, J. Quant. Spectrosc. Radiat. Transfer **27,** 437 (1982).
[17] S. N. Dobryakov and Y. S. Lebedev, Sov. Phys. Dokl. **13,** 9 (1969).
[18] W.-J. Yang (ed.), Handbook of Flow Visualisation, Chapter 20: Hesselink L. Optical Tomography, Hemisphere, New York 1989.
[19] H. Philipp, T. Neger, H. Jäger, and J. Woisetschläger, Measurement **10,** 170 (1992).
[20] W. H. Press, B. P. Flannery, S. A. Teukolsky, and W. T. Vetterling, Numerical Recipes – The Art of Scientific Computing, Chapter 10: Minimization and Maximization of Functions, Chapter 14: Modeling of Data, Cambridge University Press (1986).
[21] P. R. Bevington, Data Reduction and Error Analysis for the Physical Sciences, Chapter 11: Least-Squares Fit to an Arbitrary Function. McGraw-Hill, New York 1969.